Molecular Beam-Controlled Nucleation and Growth of Vertically Aligned Single-Wall Carbon Nanotube Arrays

Gyula Eres,*,† Anika A. Kinkhabwala,† Hongtao Cui,† David B. Geohegan,† Alexandar A. Puretzky,‡ and Douglas H. Lowndes†

Condensed Matter Sciences Division, Oak Ridge National Laboratory, P.O. Box 2008, Oak Ridge, Tennessee 37831, and Department of Materials Science and Engineering, University of Tennessee, Knoxville, Tennessee 37996

Received: March 24, 2005; In Final Form: July 11, 2005

The main obstacle to widespread application of single-wall carbon nanotubes is the lack of reproducible synthesis methods of pure material. We describe a new growth method for single-wall carbon nanotubes that uses molecular beams of precursor gases that impinge on a heated substrate coated with a catalyst thin film. In this growth environment the gas and the substrate temperature are decoupled and carbon nanotube growth occurs by surface reactions without contribution from homogeneous gas-phase reactions. This controlled reaction environment revealed that SWCNT growth is a complex multicomponent reaction in which not just C, but also H, and O play a critical role. These experiments identified acetylene as a prolific direct building block for carbon network formation that is an order of magnitude more efficient than other small-molecule precursors. The molecular jet experiments show that with optimal catalyst particle size the incidence rate of acetylene molecules plays a critical role in the formation of single-wall carbon nanotubes and dense vertically aligned arrays in which they are the dominant component. The threshold for vertically aligned growth, the growth rate, the diameter, and the number of walls of the carbon nanotubes are systematically correlated with the acetylene incidence rate and the substrate temperature.

1. Introduction

Carbon nucleation is a complex process that critically depends on a number of experimental variables including temperature, pressure, catalyst composition, and nucleation environment.[1] The exploration of new methods for synthesis of carbon nanotubes (CNT) is important because it can provide access to previously unexplored regions of this complex carbon-nucleation parameter space and lead to the discovery of new growth mechanisms and novel nanostructures.[1] Chemical vapor deposition (CVD) is regarded as the most attractive technique for synthesis of CNTs because it can be used for both device fabrication and mass production of CNTs.[2] In general, carbon nucleation and growth are dictated by kinetic processes that are specific for a particular growth method. However, all of the currently used CNT synthesis techniques, including arc discharge,[3] laser ablation of carbon,[4] and CVD[5] lack the in situ analysis and control capabilities that are needed to manipulate externally the kinetic pathways to favor formation of CNT structures with desired properties, although the potential importance of such capabilities has been recognized.[6]

Synthesis of single-wall CNTs (SWCNT) by CVD occurs by thermally induced decomposition of carbon-containing molecular species on transition metal catalyst particles (Fe, Ni, Co). Small hydrocarbons such as methane, ethane, ethylene, propylene, and acetylene and some aromatic compounds such as benzene and its derivatives are most often used as feedstock. In general, deposition of various forms of carbon occurs not directly from these molecules but from intermediate reaction products. Despite several decades of research on carbon deposition, the identity and the role of these intermediate reaction products is poorly understood. The fluid flow environment of the CVD reactor in which the mass flow and the heat flow are coupled with the reaction kinetics presents further difficulties for controlling the process.[7] Under these circumstances, the input concentration is no longer a meaningful variable. The secondary reactions can also produce undesirable side products or result in parasitic reaction sequences that are detrimental to the desired outcome of the process. The efficiency of the process and the yield of SWCNT material could be increased and a large fraction of the undesirable side products could be eliminated if a direct precursor molecule to the transformation reaction into SWCNTs could be identified. Such molecules are referred to as primary precursors. The CVD environment affords few control mechanisms and a growth environment with more sophisticated control capabilities is required to identify primary precursors. The existence of primary carbon precursors to CNT growth has not been explored. However, several decades of carbon CVD has established that certain carbon structures are more efficient in producing carbon deposits than others.[8] In this paper we describe the first use of supersonic molecular beams to identify the primary precursors to SWCNT growth, and the use and comparison of a variety of these precursors for molecular jet-induced nucleation and growth of vertically aligned (VA) SWCNTs.

2. Experimental Section

We use a high-pressure gas expansion to generate a supersonic molecular beam[9,10] of carbonaceous molecules. Because at some of the nozzle-to-substrate distances used in our experiments the gas jet collides with the substrate near the free

* To whom correspondence should be addressed. E-mail: eresg@ornl.gov.
† Oak Ridge National Laboratory.
‡ University of Tennessee.

10.1021/jp051531i CCC: $30.25
Published on Web 08/11/2005

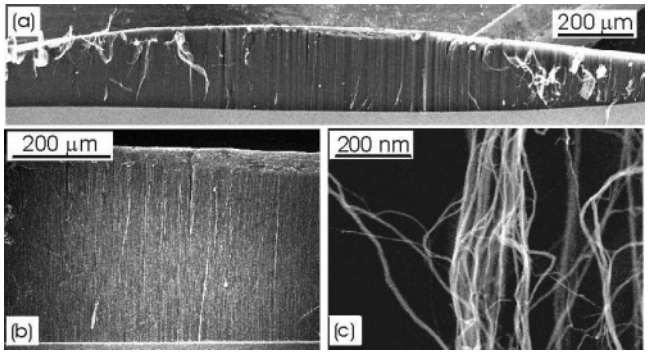

Figure 1. (a) Low-resolution SEM image of a molecular jet-grown VA-SWCNT film. The curvature in the film profile reflects the acetylene distribution in the molecular jet. The dislodged clumps of SWCNTs in the image result from the film being pulled apart after cleaving the Si substrate for edge on SEM imaging. (b) Edge on SEM image of a cleaved film at medium resolution. (c) High-resolution SEM image of a dislodged clump with individual SWCNT bundle diameters about 10 nm (the TEM image in Figure 4a shows individual SWCNTs in the bundles).

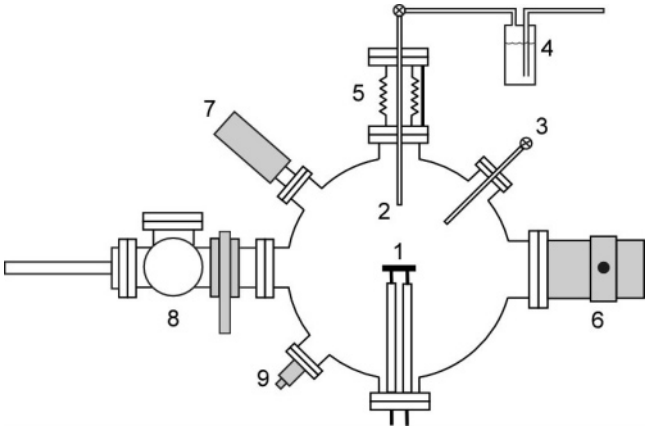

Figure 2. Schematic drawing of the experimental apparatus: (1) sample heater, (2) main molecular jet, (3) second molecular jet, (4) liquid bubbler, (5) XYZ manipulator, (6) turbomolecular pump, (7) residual gas analyzer, (8) sample transfer chamber, and (9) UHV leak valve.

molecular flow regime we refer to this molecular beam also as a molecular jet.[11] Upon collision with the surface, the C-containing molecules either chemisorb on the surface or bounce off and are pumped away. The number of molecules that undergo more than one collision with the substrate is negligible because the sample area is very small relative to the surface area of the chamber. Under these conditions, CNT growth occurs only by heterogeneous reactions from primary precursors and their direct fragments. Secondary gas-phase reactions do not contribute to CNT growth because all reaction products are scattered from the substrate and are rapidly pumped away. The cross-section SEM image of a CNT film in Figure 1 clearly reveals the outline of the incident beam profile, a feature that is characteristic of heterogeneous reactions that occur from a non-uniform spatial distribution of incident molecules.

The molecular beam apparatus consists of a stainless steel chamber that was evacuated by a turbomolecular pump. A schematic diagram of the experimental setup is shown in Figure 2. The molecular beam was generated by a high-pressure gas expansion through a 100 μm diameter nozzle orifice.[10] The source gas expansion was directed at a heated substrate containing the catalyst film. The heater consisted of a graphite filament encapsulated in a pyrolytic boron nitride disk. The sample size was 10×10 mm^2. It was attached to a sample platen and introduced into the growth chamber through a load-lock chamber. The nozzle-to-substrate distance was varied in the range from 5 to 15 mm. The reservoir pressure behind the nozzle orifice was varied in the range from a few psig to 100 psig. The incidence rate (molecules/(cm^2 s)) was determined from the measured throughput and the SWCNT film profile on the substrate.

The source gases were used in a form of a 2% mixture in 10% H_2 and 88% He. Source molecules that are liquids at room temperature were entrained in a carrier gas through a bubbler. The carrier gas consisted of a 10% H_2 and 90% He gas mixture. The presence of the source molecules in the beam was confirmed by a quadrupole mass spectrometer (Hiden, EPIC 300N) in a separate chamber. The parent ion signal was used to estimate the concentration in the beam.

Routine characterization of the deposits was performed by scanning electron microscopy (SEM) (Hitachi S4700) and Raman spectroscopy (Renishaw 1000) using the 633 nm laser wavelength. For a number of samples the Raman measurements were supplemented by transmission electron microscopy (TEM) (Hitachi HF2000) imaging.

The multilayer metal catalyst films consisting of 10 nm of Al and 1 nm of Fe were deposited by electron beam evaporation on a (100) Si wafer at room temperature. The films were characterized by X-ray photoelectron spectroscopy (XPS) (VSW, CLASS100 analyzer) prior to CNT growth.

3. Results

3.1. Source Gas Studies. A list of the molecules explored in the search for primary precursors to SWCNT growth and a summary of the results of the molecular jet growth experiments is presented in Table 1. The yield in Table 1 was scaled according to the gas composition, the Raman signal intensity, and the density of the deposit determined from the SEM images. Four of the molecules, methane, ethylene, acetylene, and propylene, are small hydrocarbons, two, benzene and xylene, are aromatic hydrocarbons, five are oxygen-containing organic compounds, and the twelfth compound is CO. The five oxygen-containing organic compounds consist of three alcohols, methanol, ethanol, and propanol, acetone, and diethyl ether. The selection of these twelve compounds was not arbitrary. The hydrocarbons were chosen because they are widely used in CNT growth by CVD.[2] Acetone was added to the list because it is a trace impurity in commercial acetylene.[12] Since our repeated attempts to remove acetone from acetylene were fruitless, we instead used growth experiments to ascertain what role acetone plays in the acetylene growth experiments. The alcohols were included because of recent reports of successful growth of single-wall and VA-SWCNTs from ethanol.[13] CO was included because it is the source gas in the HiPco process for large-scale production of CNTs.[14]

The molecular jet CNT growth experiments produced some interesting and unexpected results. All growth experiments were performed using the multilayer metal catalyst system. The small hydrocarbons, except acetylene, either produced small amounts of deposit (propylene) or no deposit (methane, ethylene) at all. The absence of CNT deposition from hydrocarbons is surprising because these molecules are routinely used in CNT CVD and CVD of other forms of carbon in this temperature range.[2,8] This trend suggests that the main pathway for C deposition from small hydrocarbons occurs through intermediates that are formed by secondary gas-phase reactions, which are suppressed in the molecular beam growth environment. The lack of deposit with benzene and xylene leads us to conclude that stepwise conden-

TABLE 1: Carbon Source Gases Used in Molecular Jet Growth Experiments

carbon source	formula	carrier gas	temp,[a] °C	deposit	MWCNT[b]	SWCNT[c]	yield	VA-SWCNT[d]
methane[e]	CH_4	10% H_2, 88% He	540−740	N				
ethylene[e]	C_2H_4	10% H_2, 88% He	650	N				
acetylene[e]	C_2H_2	10% H_2, 88% He	540−740	Y	N	Y	10	strong
propylene[e]	CH_3CHCH_2	10% H_2, 88% He	540−740	Y	Y	Y	0.1	no
benzene[f]	C_6H_6	10% H_2, 90% He	650	N				
xylene[f]	$C_6H_4(CH_3)_2$	10% H_2, 90% He	650	N				
acetone[f]	CH_3COCH_3	10% H_2, 90% He	540−740	Y	N	Y	1	weak
diethyl ether[f]	$C_2H_5OC_2H_5$	10% H_2, 90% He	650	Y	N	Y	0.5	no
methanol[f]	CH_3OH	10% H_2, 90% He	650	Y	N	Y	0.5	no
ethanol[f]	CH_3CH_2OH	10% H_2, 90% He	540−740	Y	N	Y	0.5	no
propanol[f]	$CH_3CH_2CH_2OH$	10% H_2, 90% He	650	Y	N	Y	0.5	no
carbon monoxide[e]	CO	10% H_2, 88% He	540−740	N				

[a] Temperature refers to the temperature of the substrate. [b] MWCNT = multiwall carbon nanotube. [c] SWCNT = single-wall carbon nanotube. [d] VA-SWCNT = vertically aligned SWCNT. [e] These experiments were performed in a range of incidence rates from 1.5×10^{18} to 5.3×10^{18} molecules/(cm^2 s). [f] Entrained in carrier gas using a bubbler. The beam composition is determined by the room-temperature vapor pressure.

sation of aromatic rings is not a likely mechanism in CNT growth. It appears that similarly to pyrolytic carbon deposition by CVD,[8] the benzene ring must decompose into other intermediates before CNT growth occurs.[15]

The behavior of small oxygen-containing molecules with a comparable number of C atoms as the hydrocarbon molecules is markedly different in CNT growth. In contrast to the hydrocarbons, all the oxygen-containing molecules easily produced SWCNTs. The type of bonding of oxygen to C, alcohol (−OH), ketone (═CO), or ether (−OR), where R represents an alkyl group, does not appear to be a decisive factor. The CNT growth results from the alcohol series show that the size of the alkyl group does not make an observable difference either. The common characteristic of the oxygen-containing carbon molecules is that their thermal decomposition occurs by pathways that produce oxygen-containing radicals. The mechanism by which oxygen-containing radicals enhance CNT growth could not be clarified from the results of these preliminary growth studies. We speculate that similarly to soot formation, the oxygen-containing radicals are an efficient vehicle for incorporating C through increased formation of atomic hydrogen, which promotes aromatic growth.[16]

In the HiPco process CNTs grow from C produced in a gas-phase reaction that occurs by collision of two CO molecules resulting in C and CO_2. CO is a stable molecule in surface collisions with metals and does not chemisorb and fragment readily at CNT growth temperatures.[17] Not surprisingly, molecular jet experiments produce no deposit from CO. The molecular jet experiments using CO show that the presence of oxygen alone does not ensure efficient incorporation of C into the carbon network. The use of CO (2%) along with efficient precursors such as acetylene (2%) had no effect on the outcome of the CNT growth reaction, suggesting that CO is not reactive even when active growth sites are present on the surface.

Acetylene is an order of magnitude more efficient in SWCNT growth than the nearest precursor (acetone), and it is several orders of magnitude more efficient than its hydrocarbon cousins. The molecular jet studies suggest that acetylene or acetylene-type intermediates are the principal species that react at the growing CNT surface. Numerous kinetic and mechanistic studies over the past several decades have shown that C deposition from small hydrocarbons favors the acetylene pathway.[8,18] The initial decomposition steps might be specific for different molecules, but the overall deposition reaction in a CVD environment converges to acetylene-type intermediates before C deposition occurs.

Acetone as the next most efficient precursor warrants special attention because it is an inextricable contaminant in commercially sold acetylene. For safety reasons acetylene is dissolved in liquid acetone in a ratio of 240:1.[12] The fraction of acetone present in acetylene increases as the pressure in the cylinder falls. We estimated the fraction of acetone by mass spectrometry to be about 1% in a full cylinder. We were unable to find acetone free acetylene for purchase in the US. Evidently it is available in Europe and Canada. Our repeated attempts to remove acetone by a dry ice cold trap or a filter cartridge were fruitless. The solution around this problem was to determine whether acetone enhances or hinders CNT growth. We entrained acetone in a carrier beam using a bubbler. We estimated using mass spectrometry that the concentration of acetone in a saturated carrier gas was 10%. Using the acetone molecular jet, random mats of SWCNTs were grown reproducibly. Occasionally vertically aligned bundles appeared, but the coverage was not continuous as with acetylene. That is why VA-SWCNT growth from acetone was characterized as weak in Table 1. On the basis of these measurements, we conclude that the effect of acetone on SWCNT and VA-SWCNT growth from acetylene is negligible.

3.2. Catalyst Studies. A thin film consisting of 10 nm of Al and 1 nm of Fe deposited by electron beam evaporation on a (100) Si wafer at room temperature was used as the catalyst in this work. This catalyst system has been used mainly to grow vertically aligned multiwall CNTs,[19,20] but SWCNT growth by CVD also has been demonstrated.[20,21] We note that it is a widely held assumption that the onset of CNT growth occurs after the formation of elemental Fe nanoparticles by reduction of iron oxide.[22,23] The iron oxide forms during deposition and handling, and from residual oxygen compounds present in the CVD reactor during the ramp up to growth temperature. However, the use of this catalyst system in a molecular beam growth environment revealed several unexpected trends that led to the conclusion that the active sites are related to a phase of iron oxide rather than to elemental Fe. It is important to note that heating of the sample to the growth temperature was performed in a vacuum, typically at low 10^{-7} Torr, in about 5 min. No reductive pretreatment of the catalyst films by hydrogen flow was applied. A residual gas analyzer monitoring the background composition in the chamber showed that water adsorbed on the sample platen was the main species released during heating the sample to growth temperature.

All freshly deposited catalyst films of nominally same composition produced low-density, random SWCNT mats. However, not all freshly deposited catalyst films produced VA-SWCNT growth. XPS of as-deposited catalyst films clearly shows that iron is present in the form of iron oxide.[24] The shift of the Fe peaks in the XPS spectrum depicted in Figure 3 shows that the

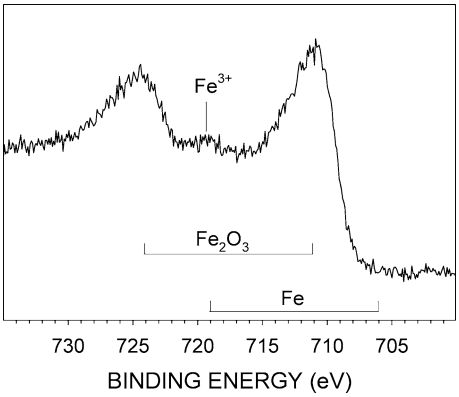

Figure 3. XPS spectrum showing the Fe 2p region. The Fe 2p core lines are shifted by ~5 eV corresponding to the Fe^{3+} state. The shake-up satellite line characteristic of the Fe^{3+} state at 719.2 eV is clearly visible.

iron oxide is Fe^{3+} rich, in agreement with the iron oxide phase diagram that shows that Fe_2O_3 is the only phase stable at room temperature in equilibrium with oxygen ambient.[25] However, no obvious difference between catalyst films that were active and those that were not active for VA-SWCNT growth could be observed by XPS. The efficacy of the metal catalyst films of the same nominal thickness and composition toward VA-SWCNT growth could be ascertained only by performing actual growth experiments. We discovered that some catalyst films became sufficiently active to produce VA-SWCNT growth after a few days exposure to ambient air. Following this observation, we were able to activate inactive catalyst films by prolonged (20−40 h) exposure to ozone generated by an UV oven. The importance of an oxidative environment for the nucleation of SWCNT growth was further confirmed by the observation that VA-SWCNT growth markedly improved with weakly active catalyst films in the presence of water vapor and oxygen. The water vapor was added in three different ways: (1) through a second nozzle; (2) through a precisely controllable leak valve; or (3) by introducing the acetylene mixture through a bubbler containing water. A 10:1 ratio of acetylene to water vapor as measured by a residual gas analyzer produced the fastest CNT growth. Oxygen was supplied as a separate beam consisting of 20% oxygen in He. The throughput ratio of the source gas to the oxygen beam was 5. In a number of experiments the oxygen beam alone with the acetylene beam or the acetylene beam saturated with water vapor alone were less effective than when both were used together. A similar catalyst system was recently studied by in situ XPS during CNT growth.[23] It was found that the Fe deposited in situ on an Al_2O_3 buffer layer was converted to Fe^{3+} during UHV annealing prior to CNT growth. Following CNT growth consisting of a 5 s exposure to acetylene, the chemical state of iron changed from Fe^{3+} to Fe^{2+}. This observation is in agreement with a detailed study of iron oxide catalyzed conversion of ethyl benzene into styrene, in which only the α-Fe_2O_3 phase was catalytically active.[26] In this process the conversion of the ethyl to the vinyl group occurs by oxidative dehydrogenation on the iron oxide surface. The spent iron oxide catalyst surface was covered with a carbonaceous deposit but reduction from Fe^{3+} to the Fe^{2+} was equally likely to contribute to deactivation of the catalyst.[26]

3.3. The Role of Acetylene Incidence Rate and Substrate Temperature. The incidence rate of acetylene was varied by changing the nozzle-to-sample distance at fixed reservoir pressure or by changing the reservoir pressure at a fixed nozzle-to-sample distance.[10] The most dramatic effect associated with the incidence rate is a transition from SWCNT growth in a form of random mats to vertically aligned growth. With optimally active catalyst films VA-SWCNT growth was observed only above a threshold acetylene incidence rate of 2×10^{18} molecules/(cm^2 s). Below this incidence rate we observe low-density SWCNT growth in a form of random mats, but free of amorphous carbon deposit and other carbonaceous side products (see TEM images in Figure 4). The distribution of acetylene molecules in a molecular jet is a complex function of the expansion conditions and the composition of the gas mixture, but in general, it is a forward peaking distribution described by a $\cos^n\theta$ function, where $n \geq 4$.[10] A $\cos^{10}\theta$ distribution that fits the cross-section SEM image in Figure 1 is fairly typical for VA-SWCNT film growth by molecular jets.[10]

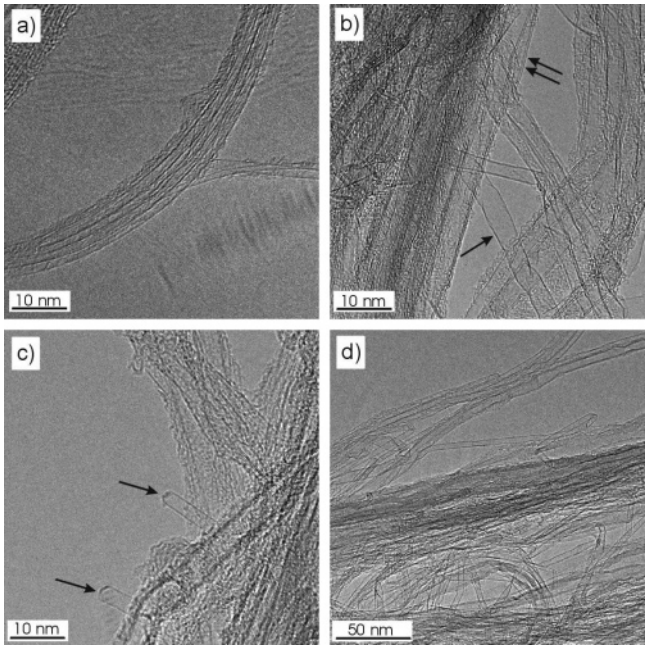

Figure 4. (a) TEM image of a SWCNT bundle from a 50 μm thick film. (b) TEM image from a 160 μm thick film showing both large diameter SWCNTs designated by a single arrow and DWCNT designated by a double arrow. (c) The arrows in this image designate two SWCNTs terminated by a cap. (d) TEM image of a large field of view showing that there are no catalyst particles attached to the nanotubes.

Raman spectra collected from the top region of the films shown in Figure 5 exhibit a clearly resolved shoulder on the G-band and strong intensity in the radial breathing modes (RBM) (see inset in Figure 5). Both features are a signature of high-quality SWCNTs.[27] The RBM peaks around 280 cm^{-1} correspond to small diameter (<0.9 nm) CNTs that could be individual SWCNTs, or these features could be attributed to inner tubes in double-wall CNTs (DWCNTs).[28] Spatially resolved Raman spectra taken in cross-section at 10-μm intervals along the length of the CNTs are shown in Figure 6. These data reveal quite clearly that the character of the CNTs changes during growth. In addition to the Raman data, TEM images show that films grown for up to 20 min (about 50 μm) depicted in Figure 4a consist of SWCNTs. Note that the catalyst remains at the substrate, i.e., the CNTs grow "from the base", and are terminated by a cap as shown in Figure 4c and not by a catalyst particle (see Figure 4d). The G to D Raman peak intensity ratio (I_G/I_D) reveals the degree of graphitic ordering,[29] and is often used as a figure of merit for evaluating and comparing the quality of CNTs from different experiments. The D-band in the Raman spectra gradually increases (see Figure 6), and the RBM

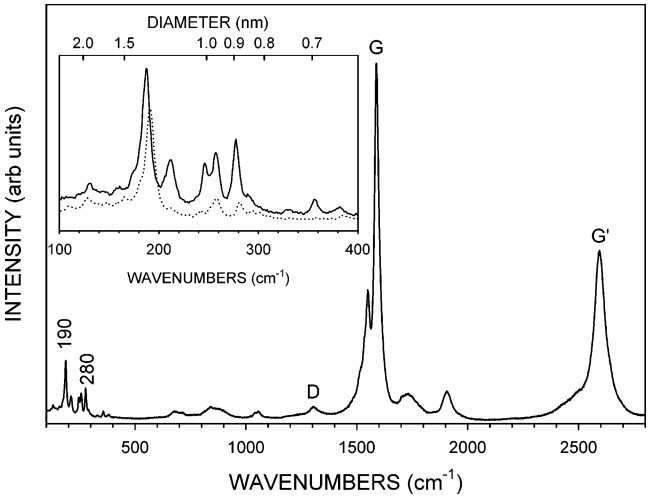

Figure 5. Typical Raman spectrum of VA-SWCNT films collected using the 633 nm laser wavelength. The main features of interest are the G-band, the D-band, and the RBMs at 190 and 280 cm^{-1}. The inset shows the enlarged RBM region of the spectra collected from the top of the films. The dotted line is for a 50 μm thick film, and the solid line is for a 160 μm thick film. The CNT diameters were calculated from $d = 248/\nu_{RBM}$. The RBM peaks of interest are the 190 and 280 cm^{-1} peaks.

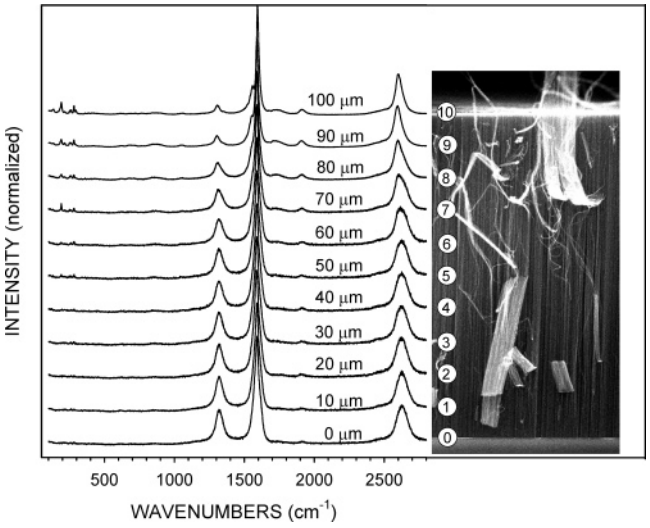

Figure 6. Spatially resolved Raman spectra as a function of film thickness. The SEM image on the right shows a 100 μm thick film. The numbers on the SEM image correspond to 10 μm steps at which the Raman spectra were collected. The substrate film interface is at the bottom (0 μm) of the SEM image.

intensity gradually falls as a function of distance from the top of the film. One way that the I_G/I_D ratio along the length of the CNTs can change is by transformation of SWCNTs into MWCNTs by forming extra outer shells. Other factors that can affect the I_G/I_D ratio include coating of the CNT walls by reaction products or amorphous carbon, and defect incorporation into the CNT walls. The TEM image in Figure 4b reveals that the thicker films contain DWCNTs along with SWCNTs.

In Figure 7 plots of the I_G/I_D ratio along the CNT length for films grown at fixed experimental conditions, but for different time durations in a range from 1 min to 4 h are shown. The individual curves collapse into a single curve (Figure 7 bottom) indicating that the evolution of thickness-dependent changes is independent of the total growth time. A common feature of the thickness plots is a change of the I_G/I_D ratio with increasing film thickness (time). The change of thickness as a function of

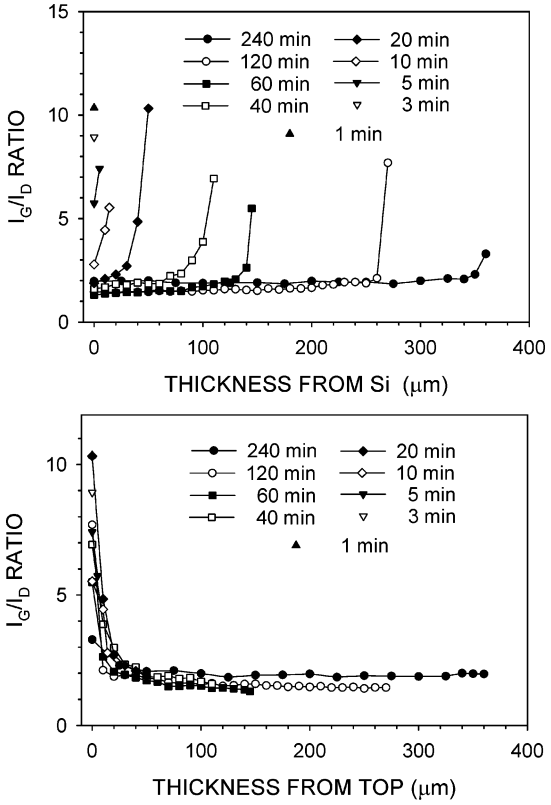

Figure 7. I_G/I_D ratio as a function of thickness for films grown at a series of growth times at 650 °C and 3×10^{18} molecules/(cm^2 s). The thickness plot from the Si surface illustrates the properties of each particular film. The thickness plot from the top shows that the changes in the bulk of the films are independent of the thickness.

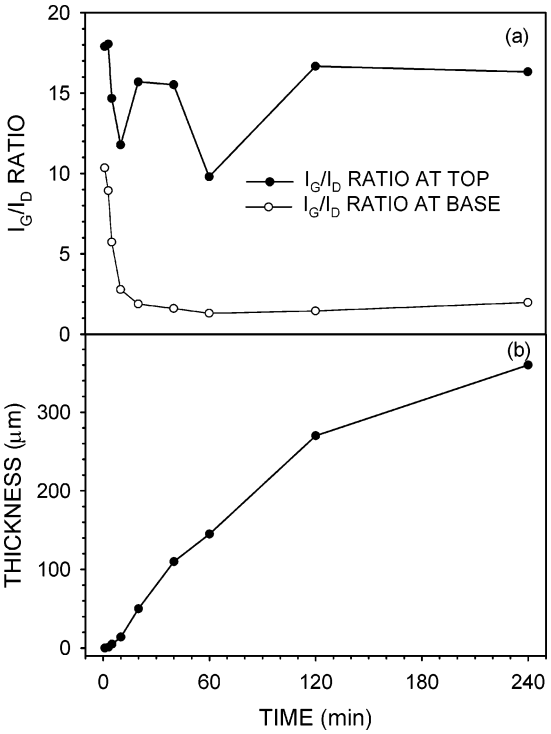

Figure 8. (a) I_G/I_D ratio derived from Figure 7 as a function of time for Raman spectra collected at the top and near the interface with the catalytic particles. (b) Plot of the thickness as a function of growth time derived from data in Figure 7.

time derived from these data is shown in Figure 8b. The growth rate curve is nonlinear and begins to saturate past 2 h of growth.

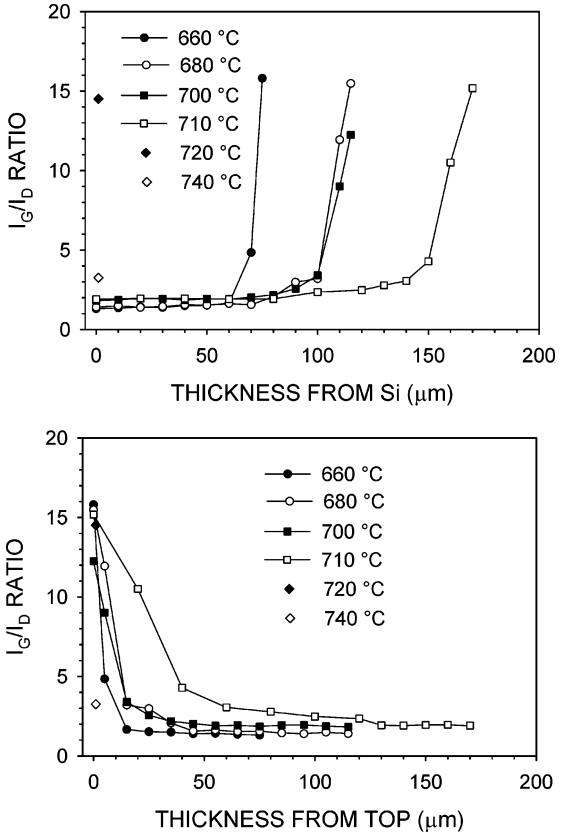

Figure 9. I_G/I_D ratio as a function of thickness for films grown at a series of substrate temperatures and a fixed incidence rate of 6×10^{18} molecules/(cm^2 s). The lines are a guide to the eye. Symbols only, represent nonvertically aligned SWCNT films. The thickness plot from the Si surface illustrates the properties for each particular film. The thickness plot from the top compares the thickness-dependent changes as a function of the substrate temperature.

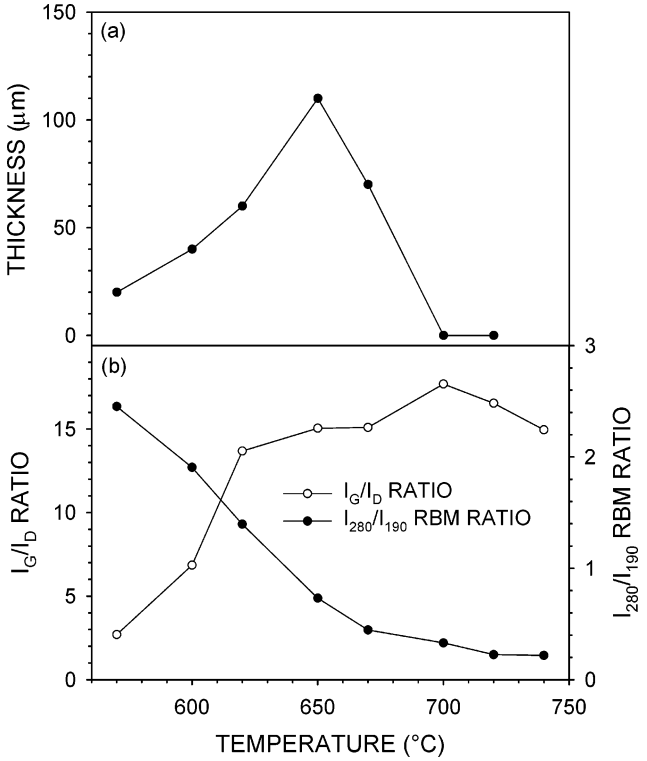

Figure 10. (a) Plot of the film thickness as a function of substrate temperature for a fixed incidence rate of 3×10^{18} molecules/(cm^2 s). (b) Plots of the I_G/I_D ratio and the I_{280}/I_{190} RBM ratio as a function of substrate temperature.

A growth rate of 2.2 μm/min was derived from the linear section of the growth curve at the onset of growth. Using this growth rate, the known incidence rate, and a value for the packing density of the CNT films of 10%, we calculate a 10^{-2} conversion efficiency of acetylene molecules. Figure 8a depicts time-dependent I_G/I_D ratios at the top and near the base of the CNTs that were extracted from the plots in Figure 7. The I_G/I_D ratio is roughly unchanged at the top of the films, but falls with growth time near the interface with the catalyst, suggesting that the active growth region is located at the base of the growing CNTs. The time-dependent data in Figure 8a are in agreement with the thickness-dependent scans in Figure 7 (bottom), which show that the change in the I_G/I_D ratio occurs within the first 30−50 μm of thickness. A change in the structure of SWCNTs in electric arc synthesized SWCNT bundles was recently reported by Loiseau et al.[30] TEM images in this work show that SWCNT bundles transform into MWCNTs near the interface with the catalytic particle surface.

The molecular beam method allows direct, systematic investigation of the effects of external growth variables such as the substrate temperature and the incidence rate of C-containing molecules on the characteristics of the CNT films. The thickness dependence of the I_G/I_D ratio at a series of growth temperatures and a fixed incidence rate of acetylene is presented in Figure 9. These curves do not collapse into a single curve revealing that the thickness evolution is temperature dependent. The plot in Figure 10a shows that VA-SWCNT growth occurs in a narrow substrate temperature window in the range from 570 to 700 °C, with the maximum growth rate at 650 °C. Interestingly, high-quality CNT growth persists past 700 °C where aligned growth ceases as the unchanged I_G/I_D ratio in Figure 10b shows. The plot in Figure 10b also shows that the ratio of the RBM peak intensity (I_{280}/I_{190}) at 280 and 190 cm^{-1} falls with increasing temperature. The interpretation of this trend depends on the assignment of the 280 cm^{-1} RBM peak. The 280 cm^{-1} RBM peak may be assigned to small-diameter SWCNTs, or to the inner tubes in DWCNTs.[28] According to this assignment, the decrease of the I_{280}/I_{190} ratio implies that large diameter SWCNTs are favored over DWCNTs at increasing substrate temperature and fixed incidence rate.[31] Alternatively, the falling I_{280}/I_{190} ratio can be interpreted as a temperature-induced shift of the SWCNT diameter distribution. A similar increase of the CNT diameters with temperature was observed in pulsed laser vaporization grown CNTs.[32]

The plot of the I_G/I_D ratio as a function of film thickness for a range of incidence rates, but otherwise fixed growth conditions is shown in Figure 11. These curves do not collapse into a single line revealing that the thickness evolution is incidence rate dependent. The plots in Figure 11 reveal that the onset of vertically aligned growth occurs at an incidence rate of 2×10^{18} acetylene molecules/(cm^2 s). Below this incidence rate high quality, but not aligned SWCNTs represented by symbols only in Figure 11 grow. Above this incidence rate the film thickness increases with the incidence rate (see Figure 12b). When the Raman signal is collected only from the top of the films, the I_G/I_D ratio increases (see Figure 12a) with incidence rate. The Raman signal from the top is representative of the SWCNTs grown in the early stages of growth and the rising I_G/I_D ratio implies that the quality of CNTs improves (higher I_G/I_D ratio) with increasing incidence rate. The most interesting trend is the increase of the I_{280}/I_{190} RMB ratio with the incidence rate depicted in Figure 12a. This trend implies that the relative fraction of small-diameter CNTs increases with the incidence

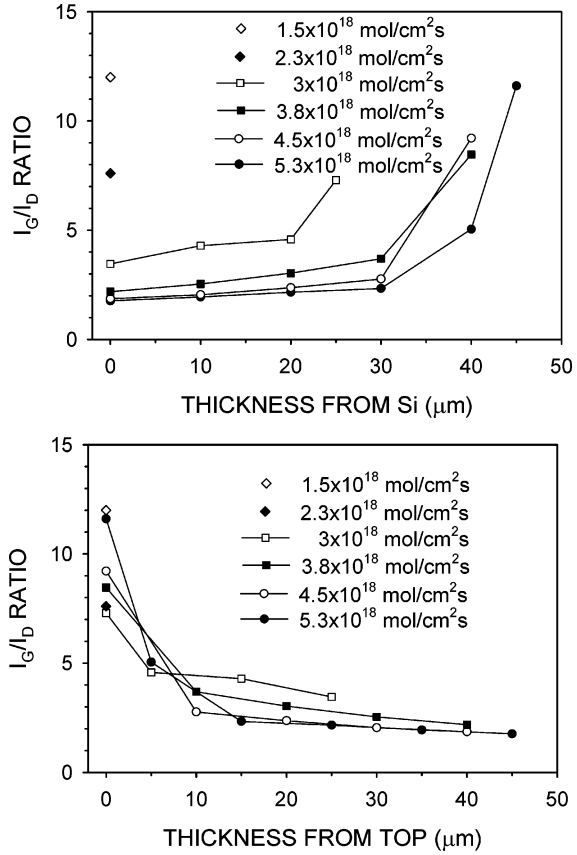

Figure 11. I_G/I_D ratio as a function of thickness for films grown at a series of incidence rates and a fixed substrate temperature of 650 °C. The lines are a guide to the eye. Symbols only, represent nonvertically aligned SWCNT films. The thickness plot from the Si surface illustrates the properties for each particular film. The thickness plot from the top compares the thickness-dependent changes as a function of the incidence rate.

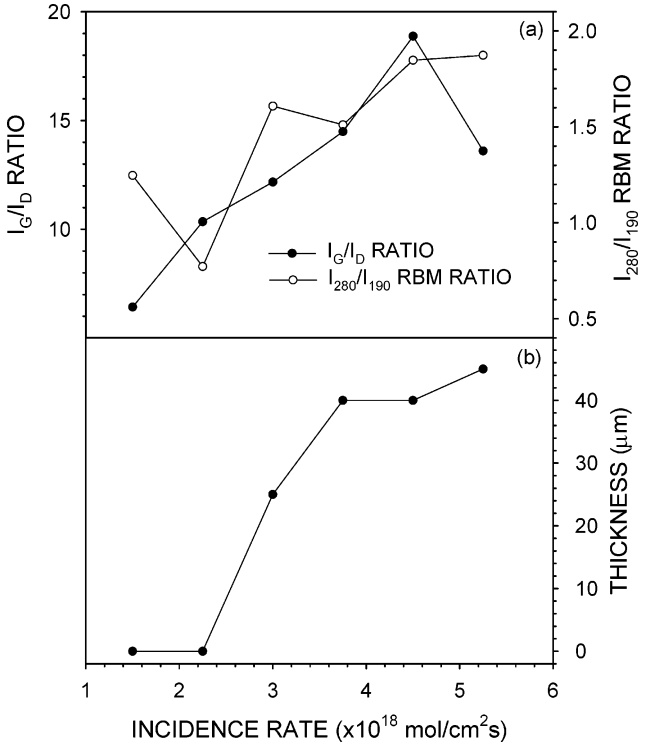

Figure 12. (a) Plots of the I_G/I_D ratio and the I_{280}/I_{190} RBM ratio as a function of the incidence rate. (b) Plot of the film thickness as a function of the incidence rate.

rate. This is a surprising observation considering that the decrease in the CNT diameters occurs at a fixed substrate temperature, a condition that is identified with constant or increasing nanoparticle size. These experimental trends demonstrate that advanced growth methods can be used to control the CNT characteristics by externally tuning the growth variables.

4. Discussion

The nature of the C-containing molecule affects the SWCNT growth kinetics through its decomposition mechanism, which is determined by its chemical composition and molecular structure.[8] The molecular beam growth experiments by suppressing gas-phase reactions reveal that acetylene provides a direct pathway to C incorporation in CNT growth. Experimental studies and theoretical modeling of soot formation in flames point to the molecular structure of acetylene as the key to efficient propagation of aromatic growth.[33] The formation of graphitic networks occurs by specific reactions unique to C_2H_2 condensation chemistry.[34] Favorable conditions for such condensation reactions to occur include the presence of radicals and hydrogen atoms that are localized on the catalyst surface or in the growing network. This reaction mechanism consisting of two steps, H-abstraction and C_2H_2-addition, is known as the "HACA mechanism".[33] The first step, abstraction of H, prepares the active site for the addition of acetylene. Molecular mass growth occurs by repeating this two-step reaction sequence, and leads to formation of polycyclic aromatic hydrocarbons (PAH). Atomic hydrogen migration along the nascent carbon network is the crucial step that enables molecular rearrangements necessary for formation of PAHs and the transformation of large molecular assemblies into three-dimensional PAHs.[33] The roles of several specific examples of hydrogen migration reactions, ring closure, interconversion of five- and six-membered rings, and migration of the cyclopenta rings along zigzag aromatic edges were explored in soot formation model calculations.[33,35] Other reactions of hydrogen migration induced rearrangements similar to these can be envisioned based on the tremendous versatility of C bonding. The initiation of aromatic ring formation may proceed through different reaction paths for different C-containing starting molecules, but the formation of large PAHs quickly converges to the C_2H_2 addition path.[33] If carbon is supplied in a form of other hydrocarbons, these molecules must first form acetylene-type species before CNT growth can occur. The similarity of the chemical pathways for soot and CNT formation can be understood if the CNTs are considered to be a form of more ordered C networks than soot.[36]

The purpose of using water and oxygen was to stabilize the iron oxide phase that catalyzes VA-SWCNT growth. The phase of iron oxide is determined by the oxidation kinetics which is governed by the growth rate and the background oxygen pressure during film deposition.[25,26] For example, low growth rates and high oxygen pressures are required to obtain Fe_2O_3. The shift of the Fe peaks in the XPS spectrum in Figure 3 clearly shows that the as-deposited catalyst films consist of Fe_2O_3. It is puzzling why films with essentially identical XPS spectra exhibit such disparity in catalytic activity. The fact that the addition of water vapor and oxygen activates inactive catalyst films suggests that there is a specific surface structure that is responsible for catalyzing the dehydrogenation reaction. Different surface terminations of Fe_2O_3 depending on the partial pressure of oxygen and water have been predicted by theoretical

calculations and observed experimentally.[37] These studies concluded that hydroxylation of certain surface orientations of α-Fe_2O_3 is strongly favored. The fact that hydroxylation occurs readily at relatively low water-to-oxygen ratios explains why even water desorption from the sample holder was sufficient to activate some catalyst films for VA-SWCNT growth. With other catalyst films addition of water was necessary to obtain the catalytically active Fe_2O_3 surface configuration.

The oxidative dehydrogenation reaction has been widely researched in connection with industrial production of styrene from ethylbenzene.[26] Hydrocarbon dehydrogenation according to a general reaction mechanism requires a concerted action of two sites, one acidic and one basic. The acidic sites on the iron oxide surface are associated with the Fe^{3+} surface or near-surface atoms and the basic sites are those of the O^{2-} sites located at step edges. The adsorption of the hydrocarbon molecules occurs at the O^{2-} sites. The hydrocarbon molecule remains attached to the surface until it is deprotonated by electron transfer to the acidic Fe^{3+} site. At each attached hydrogen site the electron transfer produces an OH and a hydrocarbon radical. If there are no nearby sites to accept the extra electron the hydrocarbon radical cannot break loose and remains attached to the surface. These hydrocarbon radicals serve as a site for molecular growth of the carbon network by addition of incoming hydrocarbon molecules. The hydrogen atoms forming the OH radicals must leave the surface for reoxidation from Fe^{2+} to Fe^{3+} to occur. The mechanism of the reoxidation reaction is not known. On the basis of bond strength arguments direct hydrogen desorption seems unlikely. It is more likely that H desorbs in a form of water removing a lattice O in the process. The role of the added water is then to restore the lattice O by dissociation of water.

Understanding the role of water and oxygen in VA-SWCTN is further complicated by the fact that both water and oxygen can also interact with the carbon-deposition process. Oxygen or oxygen-containing species are known to enhance the formation of soot and the growth of diamond[16,38] in reactions that do not require a catalyst. In soot formation the enhanced growth rates are attributed to atomic hydrogen that is formed by the oxygen-containing radical reactions. Experimental studies and theoretical models of soot formation in flames show that atomic hydrogen enhances soot growth by promoting aromatic ring formation.[16] Oxygen has been used in diamond growth in a form of molecular oxygen, water, and alcohols. Oxygen-containing species have been suggested to enhance diamond growth by producing atomic hydrogen in gas-phase reactions and by etching nondiamond carbon. A detailed experimental study of adsorption on diamond surfaces shows that atomic oxygen impinging from the gas phase is capable of breaking C−C bonds on the surface.[38] Atomic hydrogen only adsorbs at dangling bonds (2×1 reconstruction) but is not capable of breaking surface C−C bonds to produce the 1×1 reconstruction associated with the dihydride phase. The growth enhancement mechanism in diamond growth is attributed to dangling bonds that are created by oxygen radicals and serve as active sites for adsorption of carbon-containing species. Our molecular beam studies also show that oxygen-containing molecular species are more efficient source gases in SWCNT growth than the equivalent hydrocarbons with the same number of carbon atoms. Our data show no preference for a specific type of bonding between carbon and oxygen such as in alcohols, ketones, or ethers. However, a common feature of these oxygen-containing molecules is that they produce oxygen-containing radicals upon thermal decomposition. The oxygen-containing radicals can enhance SWCNT growth through mechanisms that are similar to those in soot and diamond growth.[16,38]

It was recently reported that the addition of small amounts of water into the CVD growth stream dramatically increases the growth rate of VA-SWCNTs with ethylene.[39] Because of the numerous intermediate reactions in the CVD environment, it is difficult to identify the specific oxygen-containing molecular species responsible for the growth enhancement. In our molecular beam studies we were able to control the addition of water under several different conditions, which resulted in slightly different growth results. First, it is important to point out that some catalyst films produced VA-SWCNT growth without the addition of water and that all catalyst films produced non-vertically aligned SWCNTs. We found that the addition of water strongly increased the nucleation density but only weakly increased the growth rate of the CNTs. The growth rate increase occurred at low concentrations of water and quickly saturated with additional water. As described above, the nucleation density could also be increased by increasing the incidence rate of acetylene. However, increasing the incidence rate alone could not produce vertically aligned growth with catalysts that needed water. On the basis of these observations we conclude that a specific surface structure of the catalyst is required to obtain vertically aligned growth. The addition of water with catalysts that already produced VA-SWCNT growth did not result in observable change in the CNT nucleation density or the growth rate.

The kinetic factors that affect VA-SWCNT growth can evolve spontaneously during growth, or they can be induced to change by external manipulation of the growth conditions. Subtle changes of the kinetic factors during growth affect thickness-dependent properties of the films, such as alignment, density, and CNT type. The plot of the evolution of the I_G/I_D ratio with thickness in Figure 7 shows that the onset of the changes is gradual and that the changes level off after about 50 μm. These data suggest a preference for nucleation of SWCNTs. The gradual onset of the I_G/I_D ratio change implies that the structural changes develop after SWCNTs nucleated and started growing. However, the process of nucleation and the subsequent structural changes can be accelerated under fast growth conditions as the data in Figures 11 and 12 show.

While there is great debate about the details of the mechanism of SWCNT growth, it is generally accepted that the key steps consist of formation of a CNT nucleus and the subsequent extension of the nanotube length.[40] If molecular species are used as the source of C, these steps obviously must be preceded by the fragmentation and decomposition of the C-containing molecules. The molecular structure of the C-containing molecules and their decomposition mechanisms have not been studied in CVD growth of CNTs because according to the prevailing CNT growth model the rate-limiting step is C diffusion through the molten metal particle.[40,41] The rate of SWCNT growth according to the diffusion model should increase with the temperature. The picture that emerges from our experiments is clearly at odds with (1) the models of nanotube growth that require dissolution of atomic carbon in the catalyst particles and (2) the notion that the nanoparticle size dictates the CNT diameter.[40] The fact that CNT growth is specific to acetylene suggests that the carbon-containing species do not break down to atomic carbon.

Instead, we propose a growth mechanism that is based on stepwise addition of acetylene molecules. The key pieces of experimental evidence that support this mechanism include (1) the strong specificity of VA-SWCNT growth to acetylene, (2)

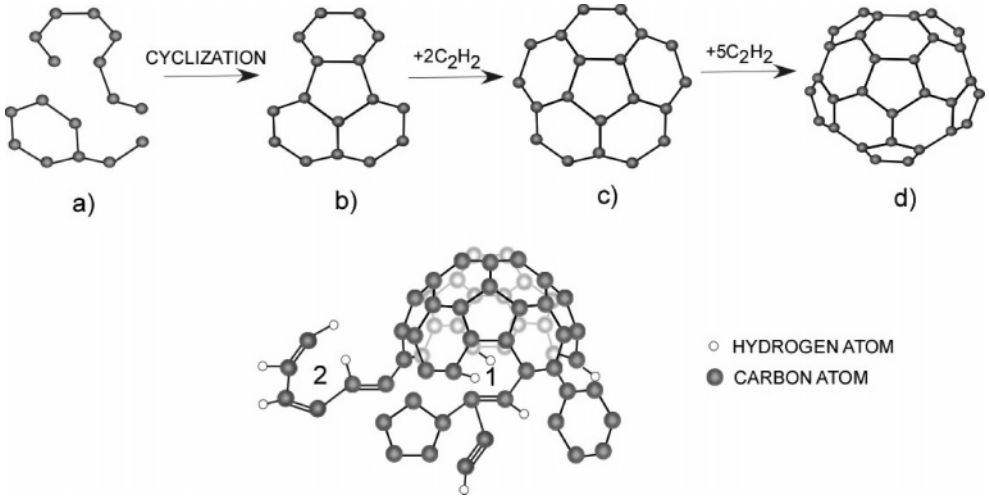

Figure 13. Schematic illustration of intermediates in formation of a nanotube cap. Flouranthene in (b) forms by cyclization from a polyacetylene chain and a small ring structure in (a). Further growth of the nucleus occurs through extension of the aromatic edges by addition of acetylene molecules. For the sake of clarity the disordered weblike network (shown in (e)) that molecular species (a)−(d) are attached to was omitted. The next intermediate is corannulene (c), followed by the CNT cap equivalent to half a buckyball in (d). After the CNT cap formed, growth occurs through the disordered weblike network that is attached to the edges of the cap (e). This pathway is reinforced by reversible decomposition of energetically less stable intermediates. The CNT cap is attached to the surface of the catalyst particle. An example of benzene ring closure after H atom migration is designated by "1". An example of formation of a five-membered ring by H_2 desorption is depicted in "2".

the anisotropic VA-SWCNT film profile, and (3) the strong dependence of the I_G/I_D ratio and the SWCNT diameter on the incidence rate of acetylene. Acetylene is known to be an essential building block in the growth of other forms of carbon including soot[33] and diamond,[42] and our molecular jet experiments show that we can add CNTs to this list. Note that in contrast to the diffusion model, which neglects the extraordinary ability of C to form complex-bonding arrangements and rearrangements, our mechanism is based on the versatility of C chemistry. The basic reaction sequence of the HACA mechanism for stepwise acetylene addition has already been discussed. This mechanism consists of the following reaction steps: H-abstraction, acetylene addition, cyclization of five- or six-membered adducts, dehydrogenation and ring closure, and intramolecular rearrangement. Maintaining efficient radical formation is the key to the continuation of this process.[33] Oxygen and OH are known promoters of aromatic ring formation by creation of atomic hydrogen.[16] We observe substantial improvement in VA-SWCNT growth especially with poorly active catalyst films when water vapor and oxygen are concurrently supplied with acetylene. The impinging acetylene molecules are catalytically dehydrogenated by the iron oxide and remain attached to the surface.[26] As more acetylene arrives, polyacetylene chains and small ring structures form by radical-type condensation reactions. The next step in this reaction sequence is the formation of a CNT nucleus. Energetic constraints dictate a curved CNT nucleus, which must consist of interconnected pentagons and hexagons.[43] Surface reactions involving collisions and subsequent bonding between acetylene, polyacetylene chains, and smaller cyclic intermediates eventually combine to form a disordered weblike structure out of which the curved CNT nuclei emerge by isomerization.[44] For a schematic illustration of possible intermediates to CNT nuclei formation see Figure 13. The proposed mechanism of CNT nucleus formation is similar to the model of fullerene formation from PAHs by stepwise addition of acetylene described by Pope.[45] The CNT nucleus must be attached to both the surface and the disordered weblike material. The length of the CNTs is extended by incorporating ribbons of hexagons along their perimeter in contact with a feeding zone, consisting of the disordered weblike material located at the base of the growing CNTs. The impinging acetylene molecules replenish the C that was incorporated into the CNTs from the feeding zone. While nucleation and the early stages of growth clearly occur by direct impingement of acetylene molecules, the later stages of growth for which direct line-of-site to the catalyst surface is obscured by the growing forest require that the acetylene molecules find their way through the growing array, with a gradual slowing of the growth rate illustrated in Figure 8b.

The presence of hydrogen atoms in the C network plays a key role in the stepwise acetylene addition mechanism. In addition to being the active sites for H abstraction, mobile hydrogen atoms enable molecular transformations such as carbon ring closure and five- to six-member ring conversion.[35] For illustration of the C rearrangement reactions in CNT growth see Figure 13. These molecular rearrangement reactions facilitate C incorporation and the extension of the CNT. Hydrogen desorption is an important step in hydrocarbon pyrolysis that has not been addressed before in context with CNT growth from hydrocarbons. The high-temperature falloff in the growth of the CNTs occurs in the temperature range where crystallization of H-saturated nanocrystalline graphite was found to expel H_2.[46] In addition to catalyst deactivation, we suggest that desorption-induced H loss is another mechanism responsible for the termination of CNT growth. The onset of H_2 desorption corresponding to recrystallization of nanostructured graphite occurs at 670 °C. Note that the rolloff in the VA-SWCNT film thickness in Figure 10a starts at 650 °C. A rising substrate temperature increases the mobility of H atoms within the carbon network and with it the probability for recombinative H_2 desorption. The amount of hydrogen present in the growing C network is determined by the dynamic equilibrium between hydrogen desorption and the acetylene incidence rate. A higher incidence rate of acetylene should compensate for H loss and shift the dynamic equilibrium and the CNT growth process toward higher temperatures. Figure 14a shows that increasing the incidence rate of acetylene shifts the CNT growth curve to higher temperatures.

The important features of the nucleation process related to VA-SWCNT film growth are the nucleation density and the

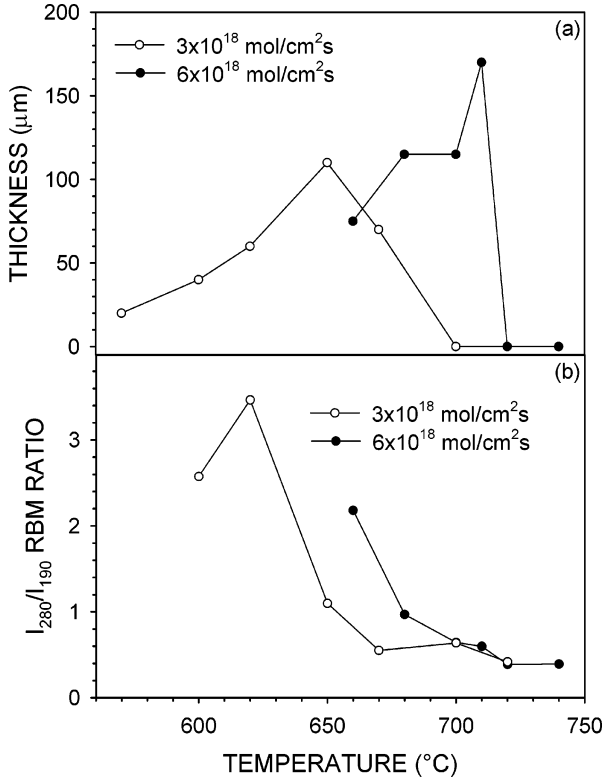

Figure 14. (a) Comparison of the temperature-dependent film thickness for two different incidence rates. (b) Plot of the I_{280}/I_{190} RBM ratio as a function of substrate temperature for two different incidence rates.

size of the individual nuclei. A higher incidence rate leads to nucleation of smaller diameter tubes even at increasing substrate temperatures as shown in Figure 14b. Note that we already showed in Figure 12a that the CNT diameters decrease with incidence rate at fixed substrate temperature. Similar behavior is characteristic of nucleation in epitaxial growth of thin films, which is described by the classical nucleation theory.[47] Elements of this theory have been used previously for calculating the nucleation density and the size of the CNT nuclei.[48] According to classical nucleation theory the size of the critical nuclei decreases and the nucleation density increases with supersaturation. The supersaturation is related to the ratio of the actual pressure in the system and the equilibrium vapor pressure of the deposit.[48] For a molecular beam the vapor pressure corresponds to the incidence rate of the growth species at the growing surface. The fact that SWCNT growth occurs directly from acetylene allows the use of molecular beams to study the incidence rate related nucleation trends in SWCNT growth. Further exploration of these trends is important because they show that factors other than the particle size can play an important role in determining the CNT diameter.

If the onset of CNT growth occurs by cap formation, then incorporation of C for the growth of the CNTs must occur at the base of the CNTs. Such a growth mechanism is commonly referred to as the root growth mechanism and it requires that the CNT tips be terminated by a fullerene cap and not by a catalyst particle. We routinely observe capped SWCNTs in our samples (see Figure 4c) by TEM imaging. In addition, the large field of view TEM image in Figure 4d corroborates that there are no particles and particle-terminated SWCNTs in our samples. Additional data supporting a root growth mechanism are presented in Figure 8a. This figure shows that the I_G/I_D ratio is roughly unchanged at the top of the growing films and that it decays at the interface with the catalyst particles. These data combined with TEM images of capped CNTs present a strong argument that the active region during growth is located at the base of the growing CNTs.

5. Conclusions

The application of molecular beams provides access to a previously unexplored region of the carbon synthesis parameter space. In addition to providing a new synthesis method for SWCNT and VA-SWCNT films, the molecular beam approach enables the separation and independent control of the most important variables in CNT growth. The temperature of the catalyst film and the impinging source gas molecules are made independent of each other by the application of the molecular beam method. This controlled reaction environment revealed that SWCNT growth is a complex multicomponent reaction in which not just C, but also H, and O play a critical role. Advanced control capabilities such as these are necessary to improve our understanding of the growth mechanisms of CNTs and ultimately will be required to control such important properties as the type, diameter, length, and chirality of the SWCNTs. A significant advantage of this pursuit is that the molecular beam growth method is compatible with the vast arsenal of surface analytic techniques enabling real time growth monitoring and property tailoring of CNTs "on the fly". The supersonic molecular jets are characterized by highly nonequilibrium translational energy, internal energy, and non-uniform spatial distribution. These nonequilibrium conditions could create interface instabilities that enhance high-density CNT nucleation.

Acknowledgment. The authors gratefully acknowledge technical assistance by Pamela Fleming. This research was sponsored by the Oak Ridge National Laboratory, managed by UT-Battelle, LLC, for the U.S. Department of Energy under contract DE-AC05-00OR22725 and the Laboratory-Directed Research and Development Program at ORNL.

References and Notes

(1) Dresselhaus, M. S. *Annu. Rev. Mater. Sci.* **1997**, *27*, 1−34.

(2) Dai, H. In *Carbon Nanotubes, Synthesis Structure, Properties, and Applications*; Dresselhaus, M. S., Dresselhaus, G., Avouris, P., Eds.; Springer-Verlag: Berlin, Germany, 2001; pp 29−53.

(3) Iijima, S. *Nature* **1991**, *354*, 56−58.

(4) Guo, T.; Nikolaev, P.; Thess, A.; Colbert, D. T.; Smalley, R. E. *Chem. Phys. Lett.* **1995**, *243*, 49−54.

(5) Dai, H.; Rinzler A. G.; Nikolaev, P.; Thess, A.; Colbert, D. T.; Smalley, R. E. *Chem. Phys. Lett.* **1996**, *260*, 471−475.

(6) Geohegan, D. B.; Puretzky, A. A.; Ivanov, I. N.; Jesse, S.; Eres, G.; Howe, J. Y. *Appl. Phys. Lett.* **2003**, *83*, 1851−1853.

(7) Smith, D. L. *Thin-Film Deposition Principles and Practice*; McGraw-Hill: New York, 1995; Chapter 7.

(8) Palmer, H. B.; Cullis, C. F. *Chemistry and Physics of Carbon*; Walker, P. L., Thrower P. A., Eds.; Dekker: New York, 1987; Vol. 1, pp 265−325.

(9) Miller, D. R. In *Atomic and Molecular Beam Methods*; Scoles, G., Ed.; Oxford: New York, 1988; Vol. I, pp 14−55.

(10) Eres G. *Crit. Rev. Solid State Mater. Sci.* **1998**, *23*, 275−322.

(11) Fenn, J. B. In *Rarefied Gas Dynamics*; Proceedings of the 13th International Symposium; Belotserkovskii, O. M., Ed.; Plenum: New York, 1985; pp 761−776.

(12) Air Products website, Safetygram-13, Acetylene.

(13) Murakami, Y.; Chiashi, S.; Miyauchi, Y.; Hu, M.; Ogura, M.; Okubo, T.; Maruyama, S. *Chem. Phys. Lett.* **2004**, *385*, 298−303.

(14) Nikolaev, P.; Bronikowski, M. J.; Bradley, R. K.; Rohmund, F.; Colbert, D. T.; Smith, K. A.; Smalley, R. E. *Chem. Phys. Lett.* **1999**, *313*, 91−97.

(15) Diener, M. D.; Nichelson. N.; Alford, J. M. *J. Phys. Chem. B* **2000**, *104*, 9615−9620.

(16) Leusden, C. P.; Peters, N. *Proc. Combust. Inst.* **2000**, *28*, 2619−2625.

(17) Brookes, N. B.; Clarke, A.; Johnson, P. D. *Phys. Rev. Lett*. **1989**, *63*, 2764−2767.
(18) Becker, A.; Hüttinger, K. J. *Carbon* **1998**, *36*, 177−199.
(19) Delzeit, L.; Nguyen, C. V.; Chen, B.; Stevens, R.; Cassell, A.; Han, J.; Meyyappan, M. *J. Phys. Chem. B* **2002**, *106*, 5629−5635.
(20) Cui, H.; Eres, G.; Howe, J. Y.; Puretzky, A.; Varela, M.; Geohegan, D. B.; Lowndes, D. H. *Chem. Phys. Lett*. **2003**, *374*, 222−228.
(21) Delzeit, L.; Chen, B.; Cassell, A.; Stevens, R.; Nguyen, C. V.; Meyyappan, M. *Chem. Phys. Lett.* **2001**, *348*, 368−374.
(22) Harutyunyan, A. R.; Pradhan, B. K.; Kim, U. J.; Chen, G.; Eklund, P. C. *Nano Lett.* **2002**, *2*, 525−530.
(23) de los Arcos, T.; Garnier, M. G.; Seo, J. W.; Oelhafen, P.; Thommen, V.; Mathys, D. *J. Phys. Chem. B* **2004**, *108*, 7728−7734.
(24) Mills, P.; Sullivan, J. L. *J. Phys. D*: *Appl. Phys.* **1983**, *16*, 723−732.
(25) Ketteler, G.; Weiss, W.; Ranke, W.; Schlögl R. *Phys. Chem. Chem. Phys.* **2001**, *3*, 1114−1122.
(26) Weiss, W.; Ranke, W. *Prog. Surf. Sci.* **2002**, *70*, 1−151.
(27) Dresselhaus, M. S.; Eklund, P. C. *Adv. Phys.* **2000**, *6*, 705−814.
(28) Bandow, S.; Chen, G.; Sumanasekera, G. U.; Gupta, R.; Yudasaka, M.; Iijima, S.; Eklund, P. *Phys. Rev. B* **2002**, *66*, 075416.
(29) Dresselhaus, M. S.; Pimenta, M. A.; Eklund, P. C.; Dresselhaus, G. In *Raman Scattering in Materials Science*; Weber, W. H., Merlin, R., Eds.; Springer-Verlag: Berlin, Germany, 2000; pp 314−364.
(30) Loiseau, A.; Gavillet, J.; Ducastelle, F.; Thibault, J.; Stephan, O.; Bernier, P.; Thair, S. *C. R. Phys.* **2003**, *4*, 975.
(31) Kim, Y. A.; Muramatsu, H.; Hayashi, T.; Endo, M.; Terrones, M.; Dresselhaus, M. S. *Chem. Phys. Lett.* **2004**, *398*, 87−92.
(32) Bandow, S.; Asaka, S.; Saito, Y.; Rao, A. M.; Grigorian, L.; Richter, E.; Eklund, P. C. *Phys. Rev. Lett*. **1998**, *80*, 3779−3782.
(33) Frenklach, M. *Phys. Chem. Chem. Phys.* **2002**, *4*, 2028−2037.
(34) Richter, H.; Mazyar, O. A.; Sumathi, R.; Green, W. H.; Howard, J. B.; Bozzelli, J. W. *J. Phys. Chem. A* **2001**, *105*, 1561−1573.
(35) Frenklach, M.; Ping, J. *Carbon* **2004**, *42*, 1209−1212.
(36) Zhang, Q. L.; O'Brien, S. C.; Heath, J. R.; Liu, Y.; Curl, R. F.; Kroto, H. W.; Smalley, R. E. *J. Phys. Chem.* **1986**, *90*, 525−528.
(37) Wang, X.-G.; Weiss, W.; Shaikhutdinov, Sh. K.; Ritter, M.; Petersen, M.; Wagner, F.; Schlögl R.; Scheffler, M. *Phys. Rev. Lett*. **1998**, *81*, 1038−1041.
(38) Thomas, R. E.; Rudder, R. A.; Markunas, R. J. *J. Vac. Sci. Technol. A* **1992**, *10*, 2451−2457.
(39) Hata, K.; Futaba, D. N.; Mizuno, K.; Namai, T.; Yumura, M.; Iijima, S. *Science* **2004**, *306*, 1362−1364.
(40) Kanzow, H.; Ding, A. *Phys. Rev. B* **1999**, *60*, 11180−11186.
(41) Baker, R. T. K.; Harris, P. S. *Chemistry and Physics of Carbon*; Walker, P. L., Thrower P. A., Eds.; Dekker: New York, 1978; Vol. 14, pp 83−165.
(42) Battaile, C. C.; Srolovitz, D. J.; Butler, J. E. *Diamond Relat. Mater*. **1997**, *6*, 1198−1206.
(43) Fan, X.; Buczko, R.; Puretzky, A. A.; Geohegan, D. B.; Howe, J. Y.; Pantelides, S. T.; Pennycook, S. J. *Phys. Rev. Lett*. **2003**, *90*, 145501.
(44) von Helden, G.; Gotts, N. G.; Bowers, M. T. *Nature* **1993**, *363*, 60−63.
(45) Pope, C. J.; Marr, J. A.; Howard, J. B. *J. Phys. Chem.* **1993**, *97*, 11001−11013.
(46) Orimo, S.; Matsushima, T.; Fuji, H.; Fukunaga, T.; Majer, G. *J. Appl. Phys.* **2001**, *90*, 1545−1549.
(47) Lewis, B.: Anderson, J. C. *Nucleation and Growth of Thin Films*; Academic: New York, 1997.
(48) Kuznetsov, V. L.; Usoltseva, A. N.; Chuvilin, A. L.; Obraztsova, E. D.; Bonard, J.-M. *Phys. Rev. B* **2001**, *64*, 235401.